1 Introduction

The invention of the transistor in 1948 by Bardeen, Brattain, and Shockley marks the advent of the semiconductor age. In retrospect, however, the most significant step was taken in 1954, when Texas Instruments introduced silicon as a substrate. This paved the way for the production of field effect transistors, which had already been proposed by Lilienfeld in 1926 and by Heil in 1934[1]: the surface of silicon can easily be oxidised to SiO_2, the very good insulating properties of which make it an ideal gate oxide. In the late 1950s, Fairchild semiconductor placed several transistors on one piece of silicon: the first integrated circuit was devised. Since then, semiconductor technology has advanced rapidly, the number of transistors per chip being doubled every 18-24 months, while the price per transistor is halved [Moo65]. Current state-of-the-art microprocessors incorporate over 100 million transistors (in 2004) at feature sizes of about 100 nm, requiring extremely complex processing technology. In a few years time, the devices will be scaled down to the size of atoms, thus limiting further integration.

Spintronics, in which conventional charge-based electronics is augmented by use of the spin degree of freedom, provides many new applications and possibilities, and possibly also answers to some challenges of the semiconductor industry. Fuelled by the industrial success of metal-based spintronic systems, such as harddisk read heads based on the giant magnetoresistance effect [Bai88, Bin89], or magnetic memory based on magnetic tunnel junctions [Miy95, Moo95], interest in the behaviour of the electron spin in semiconductor systems has grown rapidly over the last decade. Many devices have been proposed, combining the advantages of metal-based spin systems with the tunability of semiconductors [Pri95, Bal00, Wol01, Aws02]. One prominent device is the spin-transistor proposed by Datta and Das in 1990 [Das90]. Here, two spin-aligners (e.g. ferromagnets) are positioned at either end of a semiconducting channel. One spin-aligner injects spin polarised current into the semiconductor channel, through which the current passes while experiencing tunable spin-precession. The second spin-aligner detects the spin orientation at the far side of the channel. All three processes involved, spin-injection, spin-control, and spin-detection, prove to be challenging on their own. However, insight into all three processes has been gained in the last few years: spin-polarised currents have successfully been injected into semiconductors from ferromagnetic metals [Ham99, Zhu01] and semiconductors [Ohn99, Fie99]. Calculations [Ras00] and experiments [Han02] even show that the injection efficiency can be significantly increased by placing tunnel barriers at the ferromagnet/semiconductor interface. In the experiments mentioned above, optical detection of spin-polarised currents was demonstrated. Recently, even successful electrical detection of spin-polarisation has been reported [Hu01, Mei02, Ham02].

In narrow-gap III-V semiconductors, spin-precession in the semiconductor channel can be

---

[1]Julius Lilienfeld proposed a metal-semiconductor based device (MES-FET), and Oskar Heil proposed the metal-oxide semiconductor device (MOS-FET) commonly used today.

controlled via the mechanism of so-called *Rashba spin-orbit interaction* [Ras60, Ras84]: breaking of symmetry results in lifted spin degeneracy in the semiconductor channel, and the spin states $|\uparrow\rangle$ parallel and $|\downarrow\rangle$ antiparallel to a local spin-basis $\vec{B}_R$ differ in energy. While moving through the channel, an electron in the state $|s\rangle=|\uparrow\rangle+|\downarrow\rangle$ precesses around the axis defined by $\vec{B}_R$ [Das90, Ž04]. The speed of the precession depends on the so-called Rashba parameter α. Two major contributions to α can be identified, namely the electric field across the channel as well as the channel boundaries [Eng96, Eng97, Sch98]. By applying a gate voltage, the Rashba parameter can be tuned in various materials [Nit97, Hu99, Mat00, Kog02, Sch04]. In most cases, α was determined from Shubnikov-de Haas (SdH) oscillations in magnetic fields of several Tesla. However, these Rashba parameters do not necessarily agree with those at the near-zero magnetic fields, at which all proposed spintronic devices operate [Sch01, Sch02].

Weak antilocalisation (WAL) is well suited to determine the Rashba parameter at near-zero magnetic fields [Kna96, Kog02]. WAL originates from interference of time-reversed electron paths in two-dimensional electron systems. Applied magnetic fields destroy WAL, and a distinct signature in the magnetoconductance is observed which can be used to determine α. As the time-reversed paths arise from scattering, weak antilocalisation is only observed in the regime of diffusive transport. However, the interference effects causing WAL can also be used to determine the Rashba parameter at higher electron mobilities: the low-field magnetoresistance of specifically designed interferometers exhibits Al'tshuler-Aronov-Spivak (AAS) oscillations, whose amplitude depends on the strength of α [Kog04].

Tuning of the Rashba parameter is usually accompanied by a change in carrier density. Devices that, in addition to a front-gate, feature a back-gate below the channel, may provide a solution to this problem. The combination of front-gate and back-gate should enable independent control of the carrier density and the Rashba parameter [Gru00].

The work of this thesis addresses four of the topics above. First, the effect of large external magnetic fields on the Rashba parameter is investigated: the value of α is determined both by WAL and by SdH oscillations for p-type InAs single crystals and for InAs/In$_{0.75}$Ga$_{0.25}$As based heterostructures. Second, samples with ingrown back-gates are used to control the Rashba parameter independent of the carrier density. Third, the Rashba parameter is determined in low magnetic fields for a very wide range of carrier densities using WAL and AAS oscillations. Fourth, the interplay of the field and boundary contributions to the Rashba parameter are studied in samples with and without an intermediate layer at one boundary of a quantum well.

The thesis is structured as follows: the second chapter introduces spin-orbit interaction in III-V semiconductors, followed by an an overview of the effects used to determine and quantify this. Chapter 3 summarises the techniques used in sample processing and in transport experiments. Following this, Chapter 4 presents the results obtained in low and high magnetic fields on p-type InAs single crystals. Chapter 5 shows the measurements on heterostructures with an InAs channel and an ingrown back-gate. Then, in Chapter 6, measurements of AAS oscillations are shown, from which α is determined for a wide range of carrier densities. With these measurements, the interplay between the field and the boundary contribution is demonstrated for four different heterostructures with an InGaAs/InAlAs channels. This thesis closes with an outlook and conclusions in Chapter 7.

2 Basic concepts

In general, III-V semiconductors crystallise in the zinc-blende type lattice structure. Due to the inversion asymmetry of the crystal system, the spin degeneracy in the conduction band is lifted in the absence of external magnetic fields, and so-called zero-field spin-splitting occurs. This chapter gives an overview of both the physical origin of this zero-field spin-splitting in a two-dimensional electron gas (2DEG) and the phenomena used to quantify spin-splitting in transport experiments.

2.1 Zero-field spin-splitting

The spin degeneracy of electronic states in a 2DEG is lifted by breaking symmetry, either in time or in space [Rös89]. Time-reversal symmetry can be broken by an external magnetic field, resulting in the Zeeman effect [Zee97]. This thesis focusses on the breaking of spatial symmetry and the resulting so-called zero-field splitting that persists even in the absence of applied magnetic fields. The three main causes of this are the *bulk inversion asymmetry* (BIA), *structure inversion asymmetry* (SIA), and *interface inversion asymmetry* (IIA). The relative strengths of these depend on the choice of materials, dimensions, and boundaries of the channel and the 2DEG [Lom88, Ver97, Eng97].

2.1.1 Bulk inversion asymmetry

Unlike the diamond lattice structure of silicon, the zinc-blende lattice of III-V semiconductors lacks spatial inversion symmetry [Car88]. This inversion asymmetry leads to a spin-splitting that can be described by [Dre55, Pik95]:

$$\hat{H}_{BIA} = \gamma[\sigma_x k_x(k_y^2 - k_z^2) + \sigma_y k_y(k_z^2 - k_x^2) + \sigma_z k_z(k_x^2 - k_y^2)]. \tag{2.1}$$

Here, γ is a material-dependent constant[1], σ_i are the Pauli matrices and k_i the wave vectors, for $i = x, y, z$. In the case of a 2DEG, electrons are confined to a two-dimensional plane of motion. This gives rise to linear terms, in addition to the cubic ones, in the in-plane wave vector $\vec{k}_\parallel$. For confinement in direction of the z-axis this wave vector is given by $\vec{k}_\parallel = (k_x, k_y)$ and Eq.(2.1) results in [Kna96, Min04]:

$$\hat{H}_{BIA,2D} = \gamma\left[k_\parallel\left(\langle k_z^2 \rangle - \frac{k_\parallel^2}{4}\right)(\sigma_x k_x - \sigma_y k_y) + \frac{k_\parallel^3}{4}(\sigma_x k_x^3 - \sigma_y k_y^3)\right], \tag{2.2}$$

with $\langle k_z^2 \rangle$ being the mean square of the electron momentum in direction of the confinement.

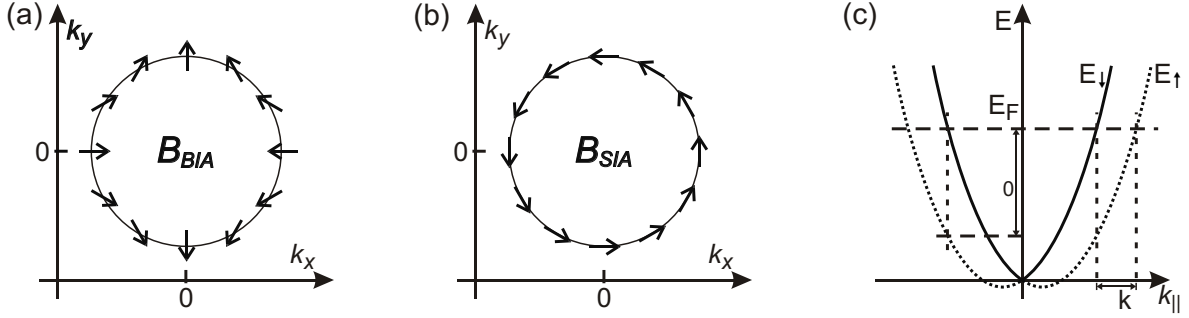[1]Some researchers refer to γ as the Dresselhaus parameter.

Fig. 2.1: Orientation of the local magnetic field caused by BIA for a 2DEG confined by a quantum well in [001] direction (a) and of the local magnetic field caused by SIA (b) according to [Win04]. Note that $\vec{B}_{BIA}$ is anisotropic in $\vec{k}_{\parallel} = (k_x, k_y)$ while $\vec{B}_{SIA}$ is not. (c) Sketch of the dispersion relations $E_{\uparrow,\downarrow}(k_{\parallel})$ in the presence of SIA. The indices $\uparrow$ and $\downarrow$ correspond to the two spin eigenstates of $\vec{B}_{SIA}$, and E_F denotes the Fermi energy. The zero-field splitting Δ_0 of the energy and Δk of the wave vector between the two spin conduction-subbands are displayed.

The above contribution to zero-field spin-splitting is often called either *Dresselhaus term* after the author of the original publication [Dre55], or *bulk inversion asymmetry (BIA)* as it stems from the bulk semiconductor lattice, or simply k^3 *term* due to the cubic order dependency on the wave vector k as is the case in bulk systems. Zero-field spin-splitting can be described by a local magnetic field that lifts spin degeneracy. The orientation of this local magnetic field is shown in Fig. 2.1(a) for the [001] plane of zinc-blende type semiconductors. From this and Eq.(2.2) it is easy to see that BIA is anisotropic in $\vec{k}_{\parallel}$ and only affects electrons with finite $\vec{k}_{\parallel}$, i.e. electrons in motion in the 2D plane.

The strength of the term linear in $\vec{k}_{\parallel}$ is influenced by γ but is also related to the thickness of the quantum well d via $\langle k_z^2 \rangle \sim d^{-2}$. As only BIA shows an explicit dependence on the thickness of the quantum well, this can be used to determine the relative strength of BIA [Luo90]. BIA is the dominant origin of zero-field spin-splitting in wide-gap semiconductors such as AlAs. With decreasing bandgap, SIA becomes dominant and BIA can be neglected as is the case for InAs or InGaAs [Sch98, Mat00].

2.1.2 Structure inversion asymmetry

The confinement of electrons in a 2DEG is generally due to a quantum well. Usually, band offsets of the boundary materials or applied voltages lead to an asymmetry of this well. The breaking of spatial symmetry results in lifted spin degeneracy, which can be exemplified as follows: the asymmetric potential well effects an electric field $\vec{\mathscr{E}} = -\vec{\nabla}\varphi$, whereby φ denotes the macroscopic electrical potential across the well. When passing through this field, the conduction electrons interact with $\vec{\mathscr{E}}$: however, due to the Lorentz transformation, $\vec{\mathscr{E}}$ appears as a magnetic field $\vec{B}_{SIA}$ when observed from the reference frame of a moving electron. The local magnetic field $\vec{B}_{SIA}$ is always perpendicular to both $\vec{\mathscr{E}}$ and to the vector of electron motion, as can be seen in Fig. 2.1(b). It can be understood as the origin of spin-splitting analogous to an external magnetic field causing the Zeeman effect. For a quantum well confined in the direction of the z-axis, the resulting spin-

splitting is described by [Ras60, Ras84]:

$$\begin{aligned}
\hat{H}_{SO} &= \alpha[\vec{\sigma} \times \vec{k}] \cdot \hat{e}_z, \\
&= \alpha(\sigma_x k_y - \sigma_y k_x).
\end{aligned} \tag{2.3}$$

In this equation $\vec{\sigma}$ denotes the vector of Pauli-matrices, $\vec{k}$ is the electron wave vector and $\hat{e}_z$ is a unit vector parallel to the electric field $\vec{\mathscr{E}}$. The spin-orbit interaction parameter α, also called the Rashba parameter, indicates the strength of the spin-orbit interaction and depends on the asymmetry of the quantum well. Assuming parabolic conduction bands, Eq.(2.3) yields the following energy dispersion relations:

$$E_\uparrow(\vec{k}_\parallel) = E_i + \frac{\hbar^2 k_\parallel^2}{2m^*} - \alpha|\vec{k}_\parallel|, \qquad\qquad E_\downarrow(\vec{k}_\parallel) = E_i + \frac{\hbar^2 k_\parallel^2}{2m^*} + \alpha|\vec{k}_\parallel|, \tag{2.4}$$

where E_i is the respective subband ground-state energy and the indices $\uparrow$ and $\downarrow$ correspond to the states $|\uparrow\rangle$ and $|\downarrow\rangle$ parallel to the two eigenvectors of the spin-basis system constituted by $\vec{B}_{SIA}$. Spin degeneracy is lifted in the absence of external magnetic fields, so SIA also contributes to zero-field spin-splitting. Fig. 2.1(c) shows a sketch of the two energy dispersions described by Eq.(2.4). The wave-vectors of the two spin orientations, $k_\uparrow$ and $k_\downarrow$, differ for any given energy, and their difference can be derived from Eq.(2.4) to be:

$$\Delta k = k_\uparrow - k_\downarrow = \frac{2m^* \alpha}{\hbar^2}. \tag{2.5}$$

The electron wave vector $\vec{k}$ is associated with the phase ψ according to $\psi \sim e^{i\vec{k}\vec{r}}$. In the presence of SIA the spin eigenstates $|\uparrow\rangle$ and $|\downarrow\rangle$ will dephase with respect to each other, and mixed states will experience spin precession. An especially interesting case occurs when the spin is of an equal superposition of the two spin basis states, i.e. $\frac{1}{\sqrt{2}}(|\uparrow\rangle + |\downarrow\rangle)$. The spin then precesses in the plane defined by $\vec{\mathscr{E}}$ and $\vec{k}$, whereby the angle of precession is given by [Dat90]:

$$\theta = \Delta k\, L = \frac{2m^* \alpha L}{\hbar^2}, \tag{2.6}$$

with L being the channel length[2]. Because the spin's precession depends on the motion of the electron through the crystal lattice, the precession is often referred to as *spin-orbit interaction*. Tunable spin-orbit interaction is necessary for tunable spintronic devices such as the spin-transistor [Dat90]. In a given device, tunability can be achieved by changing α, e.g. by changing the asymmetry of the potential well.

In the case of parabolic band structure, the Rashba parameter α also gives the correlation between the strength of zero-field spin-splitting Δ_0 and Δk, as can be derived from Eq.(2.3):

$$\Delta_0 = 2\alpha\Delta k. \tag{2.7}$$

A graphic description of these parameters is included in Fig. 2.1(c). The Rashba parameter can be described as [dAeS94, Eng96, Sch98]:

$$\alpha = \frac{\hbar^2 E_p}{6m_e} \left\langle \Psi \left| \frac{d}{dz} \left(\frac{1}{E - E_{\Gamma_7} - \varphi(z)} - \frac{1}{E - E_{\Gamma_8} - \varphi(z)} \right) \right| \Psi \right\rangle, \tag{2.8}$$

---

[2]A more extensive description of the spin precession is given in reference [Sch01].

with the $k \cdot p$ interaction parameter E_p, the free electron mass m_e, the subband energy E in the quantum well, the respective energies E_{Γ_8} and E_{Γ_7} of the valence band and the spin split-off band, and the electrical potential $\varphi(z)$. Here, the z-axis is defined as pointing from the sample surface to the substrate. When determining the derivative in Eq.(2.8), the regions of continuous potential and the boundaries between two materials must be considered separately. The so-called *field contribution* α_f to the Rashba parameter stems from the regions of continuous potential:

$$
\begin{aligned}
\alpha_f &= \underbrace{\frac{\hbar^2 E_p}{6 m_e} \left(\frac{1}{[E - E_{\Gamma_7}(z) - \varphi(z)]^2} - \frac{1}{[E - E_{\Gamma_8}(z) - \varphi(z)]^2} \right)}_{C_f} \langle \Psi | \frac{d\varphi}{dz} | \Psi \rangle \\
&= -C_f(z)\, e \langle \Psi | \mathscr{E}_z | \Psi \rangle \qquad\qquad\qquad\qquad\qquad\qquad\qquad (2.9)
\end{aligned}
$$

with the electrical field $\mathscr{E}_z = -\frac{1}{e}\frac{d\varphi}{dz}$ across the channel. Note that C_f is always negative, as $E - E_{\Gamma_7}$ is larger than $E - E_{\Gamma_8}$ for all materials, so that the sign of the field contribution is set by $\langle \Psi | \mathscr{E}_z | \Psi \rangle$. Due to the changes in band structure, the derivative in Eq.(2.8) shows a discontinuity at interfaces between different materials. Separate treatment of this derivative for the interfaces yields the so-called *boundary contribution* $\alpha_{b,i}$ to the Rashba parameter, whereby the index i indicates the respective interface at the position z_i:

$$
\begin{aligned}
\alpha_{b,i} &= \underbrace{\frac{\hbar^2 E_p}{6 m_e} \left(\frac{\Delta E_{\Gamma_7}(z_i)}{[E - E_{\Gamma_7}(z_i) - \varphi(z_i)]^2} - \frac{\Delta E_{\Gamma_8}(z_i)}{[E - E_{\Gamma_8}(z_i) - \varphi(z_i)]^2} \right)}_{C_{b,i}} |\Psi(z_i)|^2 \\
&= C_{b,i}\, |\Psi(z_i)|^2 \qquad\qquad\qquad\qquad\qquad\qquad\qquad\qquad\qquad (2.10)
\end{aligned}
$$

where $\Delta E_{\Gamma_7}(z_i) = E_{\Gamma_7}(z < z_i) - E_{\Gamma_7}(z > z_i)$ and $\Delta E_{\Gamma_8}(z_i) = E_{\Gamma_8}(z < z_i) - E_{\Gamma_8}(z > z_i)$ are the energetic changes of the Γ_7 and Γ_8 bands at the position of the boundary i and $|\Psi(z_i)|^2$ is the probability density of the electron wave function . $E_{\Gamma_7}(z_i)$ and $E_{\Gamma_8}(z_i)$ are defined as the mean values of the respective band energies on both sides of the boundary. Both field and boundary contribution must be considered to properly describe spin-orbit interaction in semiconductor heterostructures [Eng96, Gru00]. The total Rashba spin-orbit interaction parameter results as the sum of the two:

$$
\alpha_{tot} = \alpha_f + \sum_i \alpha_{b,i}, \qquad\qquad\qquad\qquad\qquad\qquad (2.11)
$$

in which the sum accounts for all boundaries i, at which the value of $|\Psi(z_i)|^2$ is not zero. The relative importance of the field and the boundary contribution can be clarified by analysing two basic potential designs, a square quantum well with differing boundary materials and $\mathscr{E}_z = 0$ as well as a quantum well with identical boundary materials but $\mathscr{E}_z \neq 0$. In the former case spin-orbit interaction can be exclusively attributed to the boundary contribution due to differing pre-factors $C_{b,u}$ and $C_{b,l}$ for the upper and lower channel boundaries [dAeS97]. In the latter case both field and boundary contributions contribute to spin-orbit interaction, whereby the field contribution dominates [Eng97, Sch98, Lin05]. In general, a full description of SIA requires consideration of both field and boundary contributions.

The description of spin-splitting becomes much more complex for non-parabolic bands. In the

simplest approach, band non-parabolicity is accounted for by using a wave-vector dependent effective mass $m^*(\vec{k})$. More refined approaches can be found e.g. in references [dAeS94, Mat00]. Zero-field spin-splitting due to an external asymmetric potential is commonly referred to as the *Rashba-effect*, caused by *structure inversion asymmetry* (SIA).

The relative strengths of the BIA and the SIA contributions to zero-field spin-splitting depend on the material system. In a rough approximation, the influence of the SIA term increases with decreasing bandgap: in III-V semiconductors with large bandgaps, e.g. AlAs[3], BIA is the main origin of zero-field splitting, whereas SIA dominates in materials with small bandgaps such as InAs[3]. For example, it has been shown theoretically that BIA is the main origin of zero-field splitting in AlGaAs/GaAs systems and that SIA dominates splitting in InAs-based heterostructures [Lom88, dAeS94]. However, of these two mechanisms, only SIA is tunable by an external parameter, e.g. a gate voltage, thus enabling control of spin-orbit interaction in a given semiconductor device.

2.1.3 Influence of boundary conditions

Recent experiments have shown that the boundaries of a quantum well have an additional influence on the strength of spin-orbit interaction. If the materials of the channel and its boundaries differ, the different compositions of constituents yield localized electric charges which are the source of *interface inversion asymmetry* (IIA) [Ver97, Kre98, Ole01]. For semiconductors with a zinc-blende lattice structure IIA is not distinguishable from BIA as the respective Hamiltonians are of the same shape [Gan03]. In fact, different strengths of IIA are observed as an enhancement or reduction of the effects typical to BIA. Therefore both effects are commonly described together using an effective combined Dresselhaus parameter γ_c that incorporates both BIA and IIA contributions [Gan04].

2.2 Shubnikov-de Haas oscillations

When a magnetic field $B_\perp$ perpendicular to a high-mobility 2DEG is varied, oscillations in the magnetoresistance are observed. The carrier density distribution of the 2DEG can easily be determined from these so-called *Shubnikov-de Haas* (SdH) *oscillations* [Shu30]. Zero-field spin-splitting commonly leads to slightly different carrier densities of the two non-degenerate spin populations. Two distinct peaks are observed in the carrier density distribution, from which the strength of the splitting can be determined. In SdH experiments, the presence of two carrier densities manifests itself as beating patterns in the oscillations [Luo88, Nit97, Mat00].

---

[3]bandgap of AlAs: 2160 meV; bandgap of GaAs: 1514 meV; bandgap of InAs: 418 meV.